

Generation of uniformly distributed dose points for anatomy-based three-dimensional dose optimization methods in brachytherapy

M. Lahanas^{a)}

Department of Medical Physics & Engineering, Strahlenklinik, Städtische Kliniken Offenbach, 63069 Offenbach, Germany

D. Baltas

Department of Medical Physics & Engineering, Strahlenklinik, Städtische Kliniken Offenbach, 63069 Offenbach, Germany and Institute of Communication & Computer Systems, National Technical University of Athens, 15773 Zografou, Athens, Greece

S. Giannouli and N. Milickovic

Department of Medical Physics & Engineering, Strahlenklinik, Städtische Kliniken Offenbach, 63069 Offenbach, Germany and Department of Electrical & Computer Engineering, National Technical University of Athens, 15773 Zografou, Athens, Greece

N. Zamboglou

Department of Medical Physics & Engineering, Strahlenklinik, Städtische Kliniken Offenbach, 63069 Offenbach, Germany and Institute of Communication & Computer Systems, National Technical University of Athens, 15773 Zografou, Athens, Greece

(Received 9 August 1999; accepted for publication 8 February 2000)

We have studied the accuracy of statistical parameters of dose distributions in brachytherapy using actual clinical implants. These include the mean, minimum and maximum dose values and the variance of the dose distribution inside the PTV (planning target volume), and on the surface of the PTV. These properties have been studied as a function of the number of uniformly distributed sampling points. These parameters, or the variants of these parameters, are used directly or indirectly in optimization procedures or for a description of the dose distribution. The accurate determination of these parameters depends on the sampling point distribution from which they have been obtained. Some optimization methods ignore catheters and critical structures surrounded by the PTV or alternatively consider as surface dose points only those on the contour lines of the PTV. D_{\min} and D_{\max} are extreme dose values which are either on the PTV surface or within the PTV. They must be avoided for specification and optimization purposes in brachytherapy. Using D_{mean} and the variance of D which we have shown to be stable parameters, achieves a more reliable description of the dose distribution on the PTV surface and within the PTV volume than does D_{\min} and D_{\max} . Generation of dose points on the real surface of the PTV is obligatory and the consideration of catheter volumes results in a realistic description of anatomical dose distributions. © 2000 American Association of Physicists in Medicine. [S0094-2405(00)01105-6]

Key words: dose distributions, dose optimization, sampling point distribution, quasi-random, brachytherapy

I. INTRODUCTION

In contrast to external beam radiotherapy dose distributions, those in brachytherapy are significantly more nonuniform. For external beam radiotherapy a few hundred sampling points can achieve an accuracy of 5%.^{1,2} This is not true for brachytherapy. To date, no systematic studies exist for the accuracy of the statistical parameters of the brachytherapy dose distribution. Brachytherapy treatment planning systems in addition to DVHs (dose-volume histograms) also give statistical parameters of the dose distribution, including the minimum and maximum dose values inside the PTV.

Sampling of dose points, both for deriving the geometrical limits of the PTV and critical structures; and for using as points to specify the dose distribution, must play a central role in the optimization procedures for modern imaging based brachytherapy.

Real 3D (three-dimensional) anatomy based multiobjective dose optimization methods³ requires the iterative calculation of dose-volume histograms (DVH) for the planning target volume (PTV), body sections and critical structures and the dose distribution on the surface of the PTV. The DVHs are usually calculated by sampling the dose distribution of a large number ($>10^5$) of uniformly distributed random points inside the PTV, and within critical structures. Other single cost function optimization algorithms include those with constraints which are related to the dose distribution, to the PTV, and to critical structures. The latest methods use sets of points distributed on the PTV surface (that is, actually on the target contours), inside the PTV volume and within the critical structures. Classical treatment planning optimization includes statistical parameters such as D_{\min} , D_{mean} , and D_{\max} and the variance, or variants of these parameters⁴⁻⁸ where D_{mean} is used indirectly.³

In some cases, such as the prostate, a critical structure, in this example the urethra, is surrounded by the PTV volume giving a PTV that is not continuously filling the anatomical volume enclosed by the PTV outer contours. In such cases, points generated inside the 3D PTV contour surface must be ignored if they are within any critical structure. In addition, any points inside the PTV, critical structures and any tissue volume, which are also inside the catheters, should be ignored. These constraints are not incorporated within any current brachytherapy software.

The constraints are implemented by avoidance of points closer than a given distance to the catheters, which is determined by the outer radius of the catheters. It could also be a clinical decision to ignore small volumes adjacent to the catheters by specifying an additional margin to the physical catheter outer radius.

The main aim of some dose optimization algorithms is that a defined isodose surface should ideally conform to the shape of the PTV. Usually this shape is described by a set of sampling points and the algorithms try to minimize the variance of the dose values at these dose points. To accurately describe the 3D shape of the PTV surface, the sampling points have to be uniformly distributed on its surface. However, some methods which are based on the estimation of the minimum peripheral dose (MPD) or the equivalent of the minimum target dose (MTD),⁹ and which use dose points distributed on the PTV contours as a representation of the 3D PTV surface, could give biased results, since they do not obviously cover the whole PTV.

Points inside the PTV and critical structures are used for the calculation of the volume which is required for the normalization of the DVHs, and this can be achieved with a high accuracy by a simple Monte Carlo integration technique. Due to the high dose gradients, many more sampling points are generally required in brachytherapy for the accurate calculation of DVHs than in external beam radiotherapy.

We present in this paper a number of new algorithms for the efficient generation of dose points which are uniformly distributed on the surface of the PTV; firstly within the PTV, and also within organs at risk or other tissues of interest where the constraints relate to catheter location and diameter. The 3D anatomical volumes are represented by sets of cross-sectional contours. The results of implementation of these algorithms in a range of clinical implant situations are presented and discussed, and the benefits of the new algorithms are described.

II. METHODS

In this section a method is presented which generates sampling points inside a triangulated surface of the PTV and other objects. This includes the exclusion of volumes inside sources or catheters. Additionally a method is presented which generates sampling points on the whole surface of the PTV.

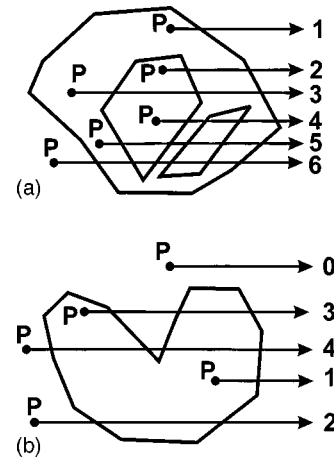


FIG. 1. Schematic diagram illustrating a generalized point P in relation to a 2D cross section through a polygon (a) with and (b) without a critical structure inside the cross section. The number of intersections is shown for each point.

A. Points within a volume

We assume that every volume is represented by planar contours which are obtained from parallel cross-sectional images using either CT (computed tomography) or MRI (magnetic resonance imaging). We also assume that when using the planar contours of a volume, its surface is represented by triangles using triangulation procedures such as described by Fuchs *et al.*¹⁰ or Boissonnat *et al.*¹¹ The triangulation is assumed to cover the whole surface, including the surface of both ends of the object.

The catheters are considered as a special category of nonanatomical 3D objects and are defined as a list of *catheter describing points* in 3D space as described by Tsalpatouros *et al.*¹² and by the catheter outer radius with or without an additional clinical margin. For catheters with a typical very small outer radius of 1 to 2 mm, the triangulation is not a suitable method for reconstruction of the volume surface. Because of their typical cylindrical geometry the surface and the volume encompassed by the catheters is determined analytically.

The verification procedure consists of determining whether a point is inside the volume as described by the planar contours and its triangulated surface. The basic part of this procedure is essentially reduced to a 2D verification of whether a point is inside a given contour on a given plane.

1. Test of if a point is within a 2D contour

We consider a 2D contour as a closed polygon made up of N vertices $(x_i, y_i)_{i \in 1, \dots, N}$. There are several methods which can prove if a point $P = (x_p, y_p)$ is within such a polygon but the most efficient method is the topology-based method. In order to determine if a point P is inside the polygon we consider a horizontal ray emanating from P towards the right, see Fig. 1.

We count the number of intersections of a ray with all edges of the polygon. If the number of edges of the polygon intersected by the ray is even then the point P is outside the

polygon, and if the number of intersections is odd then the point P lies inside the polygon. This is a consequence of the Jordan curve theorem in topology and a proof is given by Courant *et al.*¹³ There are some special cases when a ray passes exactly through a vertex. These situations can be considered using tie breaking rules or by a method such as described by Edelsbrunner *et al.*¹⁴

2. Test of if a point is within a volume

We have to determine whether a point is inside or outside a volume. The previously mentioned 2D algorithm for a test of a point inside a polygon can be extended to a test for a point inside a polyhedron. Due to the very high number of triangles, that is facets of the polyhedron, such a method would be computationally very inefficient. For this reason we use the following procedure to check if a point P with coordinates (x_p, y_p, z_p) is inside the triangulated surface of a volume. We assume that the planar contours of the volume are parallel to the z axis and in the range $[z_{\min}, z_{\max}]$. We test if the point is inside the bounding box described by the contours. If the result is positive then the point is between two image planes containing these contours: $z_p \in [z_{\text{before}}, z_{\text{after}}]$.

In cases where the point under consideration lies on a plane containing the contour, we set the default as $z_{\text{before}} = z_{\text{after}} = z_p$. We then test if the point is in the plane at $z = z_{\text{before}}$. If the result is positive we test if it is inside the corresponding 2D contour. Otherwise, $z_p \neq z_{\text{before}}$, we test the projections of the point on the cross-sectional planes at z_{before} and z_{after} relative to the volume contours in these planes.

If the projections of the point are inside both planes then the point is considered to be inside the volume, or if they are outside both planes then the point is considered to be outside the volume. If this is not the case which is relatively rare, then the object contour at $z = z_p$ is calculated by interpolating between the object contours at $z = z_{\text{before}}$ and $z = z_{\text{after}}$ and in a further procedure, it is verified whether the point is inside or outside the interpolated contour. This contour is obtained from the intersection points of the triangles of the triangulated object surface and a plane perpendicular to the z axis at $z = z_p$, that is, through the point.¹⁵

An additional test is then necessary to avoid the possibility that the point is at the same time inside any other contoured volume. An exception is the case when the volume under consideration is what we term *the body*. This includes the PTV, normal tissue and critical structures.³

If this test succeeds, a final test is required to verify if the point is outside any of the catheters. If this result is positive, then the point is finally considered to be inside the volume of interest. The flowchart for our algorithm is given in Fig. 2.

3. Test of if a point is outside a catheter

Various optimization methods require a knowledge of the average or maximum dose value that is within a given volume such as the PTV or various critical structures.^{7,8} If in addition the optimization objective is a homogenous dose distribution within the PTV,⁵ then the variance of the dose

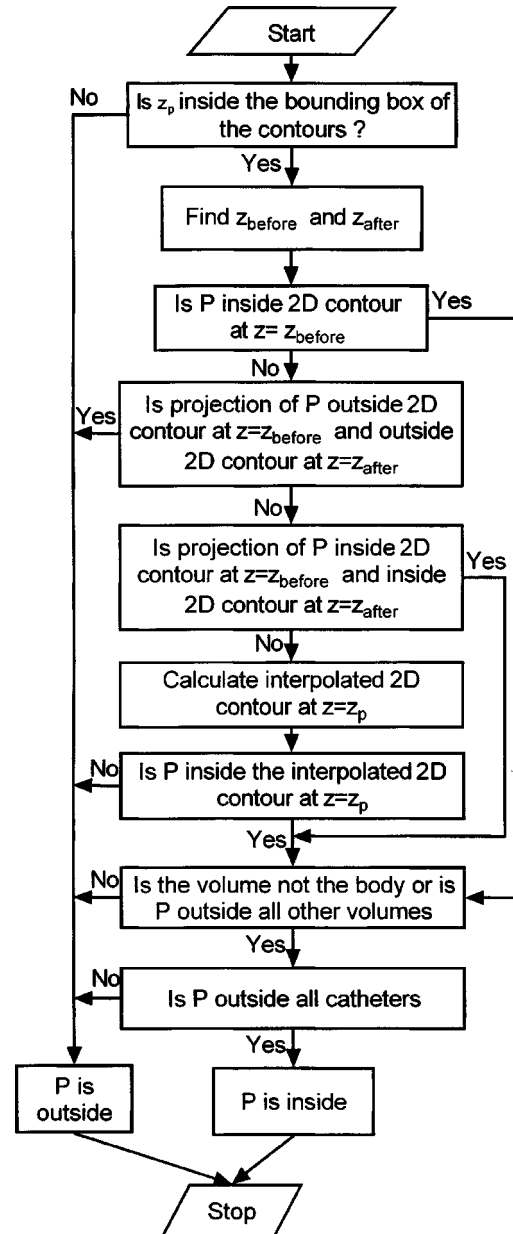


Fig. 2. Flow chart of the algorithm for the generation of dose points inside a volume.

value distribution inside PTV has to be minimized. There is always a problem if dose points are produced within the catheter volumes which result in very short distances from the sources or even lying exactly at sources positions. The dose values at these points are very high and depend on the dwell weights assigned to the source dwell positions. These very high dose values cause wide fluctuations in the mean and maximum dose values and the corresponding χ^2 values. These fluctuations must be reduced as much as possible.

This could theoretically be avoided by using a specific cut-off maximum dose value. The disadvantages of such a method is that in the iterative process it is not known which parts of a volume are excluded in the optimization process and that the cut-off value is an arbitrary value. Another method of avoiding the numerical difficulties due to the pres-

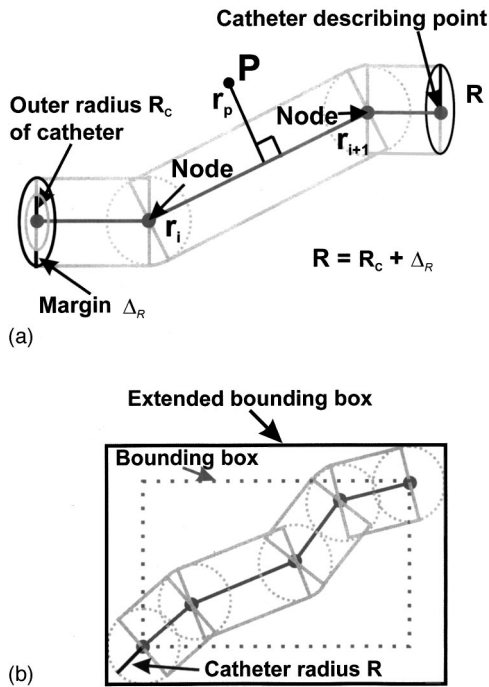


FIG. 3. (a) Schematic diagram of the parameters required to test if a point is inside a catheter with an outer radius R_c and margin Δ_R . (b) Schematic diagram of a bounding box. This is shown only for a single catheter but in practice the box would include all catheters.

ence of singularities is the use of the *harmonic peripheral dose* (HPD) proposed by Yu.¹⁶

Both these methods deal with a problem in a manner which is not logical with regard to clinical practice. It makes no sense to calculate doses within a radioactive source or within catheters since these are nontissue volumes. A more logical approach is the exclusion of dose points lying inside the source or the catheters. Because of this we have to test if a point is outside a catheter.

We assume that catheters are curved cylinders which can be approximated by cylindrical segments connecting sequential catheter describing points¹² and spheres centered at the nodes: These are catheter describing points belonging to two sequential segments, see Fig. 3(a). Given the outer radius R_c of a catheter, points closer than $R = R_c$ from every catheter segment and node must be excluded. In order to test if a point is inside a catheter we calculate the minimum distance between the point and any catheter segment. If it is smaller than R then this point is inside the catheter and has to be excluded.

The clinical *margin* Δ_R specified by the physician, can be expressed as an additional shell surrounding the catheter resulting in a corresponding increase of the effective catheter outer radius increasing this to R where $R = R_c + \Delta_R$. For the catheter types (microSelectron HDR, Nucletron B.V., Veenendaal, The Netherlands) we use clinically, there is a distance of 5–10 mm between the catheter tip and the first possible source dwell position within the catheter, depending on catheter type. Knowing that the first catheter describing point is adjusted to describe the catheter tip there is no need

for our catheters to define an additional margin to the tip of the catheters.

Firstly, verification is carried out to determine if a dose point P is within any of the spheres centered at the catheter nodes, Fig. 3(a). If this is the case, then the point is inside the catheter: Otherwise the following procedure for the cylindrical segments is initialized.

Given that the equation of the line for a catheter segment through the sequential catheter describing points r_i and r_{i+1} is:

$$r(u) = r_i + u(r_{i+1} - r_i), \quad (1)$$

then the minimum distance of a dose point P at r_p and the segment is at the point $r(u_{\min})$ where $r_p - r(u_{\min})$ is perpendicular to the segment, Fig. 3(a). Therefore using Eqs. (1) and (2) we obtain for the point $r(u_{\min})$

$$(r_{i+1} - r_i) \cdot (r_p - r(u_{\min})) = 0, \quad (2)$$

$$u_{\min} = (r_p - r_i) \cdot (r_{i+1} - r_i) / \text{dist}(r_i, r_{i+1})^2, \quad (3)$$

where $\text{dist}(r_i, r_{i+1})$ is the Euclidean distance between r_i and r_{i+1} . If $u_{\min} \notin [0, 1]$ then the point $r(u_{\min})$ is not on the segment between r_i and r_{i+1} but on one of its extensions and r_p is considered to be outside this segment. If $u_{\min} \in [0, 1]$ then we calculate the distance of the point r_p and the line segment $\text{dist}(r_p, r(u_{\min}))$. If $\text{dist}(r_p, r(u_{\min})) < R$ then the point is considered to be inside the catheter and a test for the other segments is omitted.

The length of each catheter segment $\text{dist}(r_i, r_{i+1})$ is the most computational time consuming operation in Eq. (3) and, therefore, is calculated only once in a pre-processing step and the value of $1/\text{dist}(r_i, r_{i+1})^2$ is stored.

It is not necessary to calculate for every dose point its distance from all catheter segments. The calculation procedure can be minimized by incorporating in the algorithm the coordinates which define the limits of the catheter segments, and extending these limits by a distance by R in each direction: This defines what we term the *bounding box*. A test is then necessary to determine whether any dose points are within this bounding box. If they are outside the box then they are obviously not within a catheter. If they are within the box then it must be verified that they are not within a catheter, Fig. 3(b). Using this algorithm, which is not complicated, the test inside a catheter requires only a few seconds for 100 000 sampling points.

4. Generation of points within a volume

Using the previously described algorithms we can generate sampling points inside an object. We produce points inside the bounding box of the object and test using our algorithm if they are inside the volume. The sampling points inside a volume are generated using triplets of Sobol sequences. These are known as quasi-random sequences (QR): Deterministic low discrepancy sequences LDS, which fill the 3D space more uniformly than uncorrelated random points. We use the Numerical Recipes Routine *sobseq* which produces Sobol sequences.¹⁷ Obtaining these sequences does not significantly lengthen the computing time compared with a

time to produce the same number of pseudorandomly distributed sampling points using standard routines. It is also known that Monte Carlo integration using QR converges faster than using pseudorandom distributed sampling points.^{1,2,17}

The use of an aligned minimum bounding rectangular box¹⁸ of the volume can further increase the speed of the generation of points inside the object. The production of points inside the minimum bounding box will increase the efficiency of the procedure by reducing the probability of generating points outside the object. This effect becomes very significant if the main axes of the object are not aligned with the coordinate system in use.

B. Points on the surface of a volume

Some dose optimization methods use points on the surface of PTV and optimize the dose distribution by requiring that a given isodose surface should ideally conform to the shape of the PTV. For these methods several disadvantages can occur as follows. Dose points are considered to be equidistant only on the contour lines of PTV,^{4,5} see Figs. 4(a) and 4(b).

No dose points exist which are lying at the superior and inferior ends of the PTV. If the points are limited to the contours then increasing their number will not significantly improve the accuracy of the calculated dose distribution on the surface, even if there is convergence to some values for the variance of the mean, for the minimum and for the maximum dose values. This does not necessarily represent the true dose values on the whole surface of the PTV. The lack of dose points on the major part of the surface of the PTV and the restriction of dose points on its contour lines is a severe limitation if the quality of the optimization relies on the variance on the surface dose distribution. If the distance between the contours is large and there is a significant change in the shape and size of the contours from plane to plane, then the dose distribution derived from the dose points on the contour lines inaccurately represents the true dose distribution on the surface.

One approach is to use sampling points on interpolated contours. However, this method is computationally complex and requires the calculation of new contours if one wants to increase the number of sampling points on the surface of the PTV. A different method has to be used to fill the two ends of the PTV with sampling points.

There is in the current literature in general no analytic method known for producing uniformly distributed points on the surface of an object as for example in the special case of a spherical object where points uniformly distributed on the surface of the sphere can be produced by the following algorithm.

Choose a random number s uniformly distributed in $[-1,1]$ and a random number ϕ uniformly distributed in $[0, 2\pi]$. The x , y and z coordinates of the point are given by:



(a)



(b)

FIG. 4. Dose points produced equally spaced (a) on the contour lines and (b) on the surface of PTV for the cervix implant. The total number of points is the same in both cases. The dose points on the surface of the PTV have been produced using barycentric triangle coordinates and the Stochastic Universal Sampling (SUS) algorithm.

$$x = r \cdot \sqrt{1 - s^2} \cdot \cos(\phi),$$

$$y = r \cdot \sqrt{1 - s^2} \cdot \sin(\phi),$$

$$z = r \cdot s.$$

The principle underlying this algorithm is that for a sphere of radius r , the area of a zone of width h is always $2\pi rh$, regardless of where the sphere is sliced. Therefore, the z coordinates of random points on a sphere are distributed uniformly. Points obtained by using this algorithm are then uniformly distributed on the surface of the sphere.

We have developed a simple method to generate points randomly and homogeneously distributed on the entire sur-

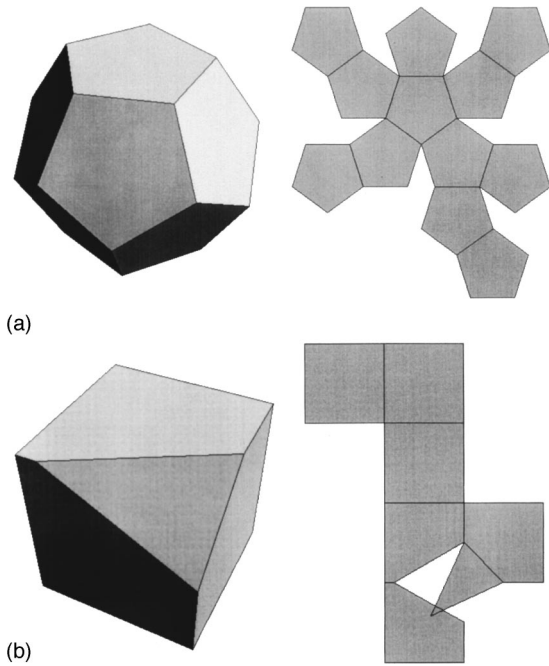


FIG. 5. (a) Dodecahedron and its unfolded surface. (b) A self-overlapping unfolding of a polyhedron which is a truncated cube. The dodecahedron and the truncated cube have been obtained using a Mathematica notebook of Namiki and Fukuda (Ref. 19).

face of a volume described by contours. A triangulation of the volume is assumed.

1. Generation of points on the surface of the PTV

We assume that the surface of the PTV is approximated by a triangulation of the contours describing the PTV with the triangles of the PTV surface forming a polyhedron. The logical idea to produce uniformly distributed points on the unfolded surface of this polyhedron and then to fold it back with the distributed points is in general not possible. For a convex polyhedron P with e edges and f faces unfolding of P is defined as a planar cell complex obtained from the boundary complex of P by cutting $e-(f+1)$ edges of P and bending it along the remaining edges,¹⁹ Fig. 5(a).

There is no method known for unfolding non-convex objects and even for very simple convex polyhedra there is a possibility that the unfolding produces a self-overlapping planar complex,¹⁹ Fig. 5(b). In order to overcome this limitation, we have developed a method which replaces the explicit folding described by a surface mapping method, that could be considered as an indirect folding procedure, and which can be applied for any type of 3D objects and surfaces.

Our method assumes that the surface of the object is triangulated. Triangles of the surface are then selected with a probability proportional to their area. Then uniformly distributed random points are produced inside the selected triangle.

If $v_1, v_2,$ and v_3 are the three vertices of a triangle T then its area A is given by

$$A = 0.5 |(v_2 - v_1) \times (v_3 - v_1)|.$$

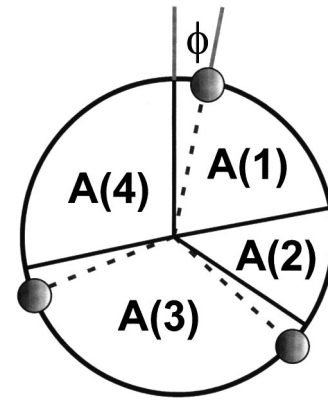


FIG. 6. Example of the production of three dose points on the surface of a tetrahedron with the SUS algorithm. We have four triangles and we select the triangles using the three markers which are denoted by open circles: By one times triangle 1 and two times triangle 3. Each time a triangle is selected a random point is generated inside it.

Our aim is to generate uniformly distributed points on the object surface. Because of this the Stochastic remainder sampling, that is, *roulette wheel selection*²⁰ is not the appropriate selection method because as already proved, this method is biased for a low number of points.²¹ We decided to produce a point on a surface using the Stochastic Universal Sampling Algorithm (SUS).²¹ We assign for each triangle obtained by the triangulation of the PTV surface a sector on a circle covering a fraction of the total circle area equal to the fraction of the PTV surface that is represented by the area of the triangle. On the periphery of the circle N equally distributed markers are set, where N is the number of points we want to generate on the PTV surface. All the markers are rotated by the same random angle ϕ on the circle periphery which will guarantee that on the average each triangle is selected with the appropriate probability independently of the sample size. At the end the number of markers lying inside the different sectors corresponding to the available triangles is recorded. Figure 6 shows a schematic representation of the SUS algorithm²¹ for a tetrahedron with four triangular facets. The length of the circumference of each sector $A(1)$ - $A(4)$ is proportional to area of each triangle. The number of markers falling into each triangle is on average proportional to the length of each sector corresponding to the triangle.

Thereafter in each triangle a number of randomly distributed points is generated equal to the number of recorded markers within the corresponding circle sector according to the following procedure.

If t_1, t_2, t_3 are real numbers $\in [0,1]$ so that their sum is: $t_1 + t_2 + t_3 = 1$ then the point

$$P = t_1 \cdot v_1 + t_2 \cdot v_2 + t_3 \cdot v_3, \tag{4}$$

lies on the plane of triangle T with the vertices $v_1, v_2,$ and v_3 and is inside this triangle. The numbers (t_1, t_2, t_3) are called the *barycentric coordinates* of P with respect to T . Any point P inside the triangle can be expressed uniquely by Eq. (4). In principle there are only two independent random numbers, the barycentric coordinates t_1 and t_2 , and these are

TABLE I. Characteristics of the five clinical implants.

Implant site	PTV (cm ³)	PTV surface (cm ²)	Number of catheters	Catheters per cm ³	Number of dwells positions	Dwell positions per cm ³	Number of dose points	Catheter material
Neck	17.7	40.7	5	0.28	51	2.87	1481	plastic
Prostate	20.7	50.3	4	0.19	20	0.96	665	metallic
Breast	123.1	142.4	10	0.08	219	1.78	1954	plastic
Cervix	221.4	228.7	9	0.04	162	0.73	1404	metallic
Rib	504.0	421.4	12	0.02	177	0.35	2838	plastic

used to generate a random point inside a triangle T . The third barycentric coordinate t_3 is then calculated by $t_3 = 1 - t_1 - t_2$. If $t_1 + t_2 > 1$, then t_1 is replaced by $1 - t_1$ and t_2 by $1 - t_2$. Using Eq. (4) we then obtain the random point P inside T .

Points generated inside a triangle with this method are uniformly distributed. Since the triangles are selected with a probability proportional to their area the points on the triangulated surface will also be uniformly distributed, Fig. 4(b). As in the case of the volume, we also have for a surface that the points which are generated are accepted only if they are not inside catheters or inside structures.

III. MATERIAL

The material used in this study are five real clinical implants and not theoretically devised examples. They represent a typical clinical range of PTVs from <20 cm³ to >500 cm³, of 4–12 catheters and of 20 to >200 dwell positions, see Table I.

A. Neck implant

This example is a small volume lymph node implant in the neck with a PTV volume of 17.7 cm³. The 3D PTV contours and the source dwell positions within the catheters are shown in Fig. 7.

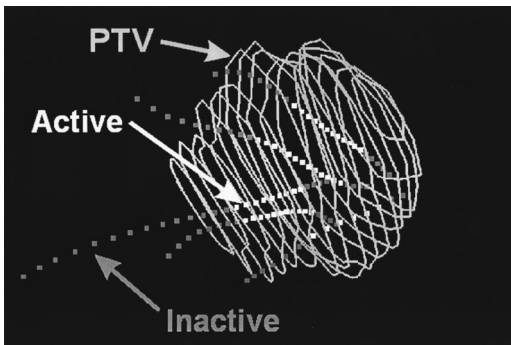


FIG. 7. 3D contour lines of the PTV with the source dwell positions within the five flexible plastic catheters of the head and neck implant. The active dwell positions inside the PTV which have been selected for the treatment planning are of a minimum distance of 5 mm from its surface.

B. Prostate implant

This example is a prostate implant made with a PTV volume of 20.7 cm³. The 3D PTV contours and the source dwell positions within the catheters are shown in Fig. 8.

C. Breast implant

This example is a breast implant made with a PTV volume of 123.1 cm³. The 3D PTV contours and the source dwell positions within the catheters are shown in Fig. 9.

D. Cervix implant

This example is a cervix implant made with a PTV volume of 221.4 cm³. The 3D PTV contours and the source dwell positions within the catheters are shown in Fig. 10, see also Fig. 4.

E. Rib implant

This example is a rib implant made with a PTV volume of 504 cm³. The 3D PTV contours and the source dwell positions within the catheters are shown in Fig. 11.

IV. RESULTS

A. Dose points on the PTV surface

Our study has involved calculating the dose on the PTV surface using only dose points on the PTV contours and then using only dose points on the PTV surface. A comparison of these results is made with a reference which is the normal

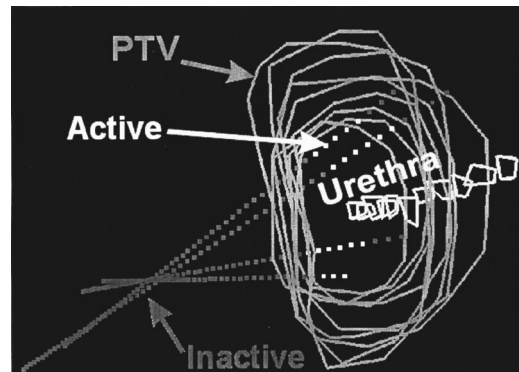


FIG. 8. 3D contour lines of the PTV for the prostate implant including the urethra as a critical structure.

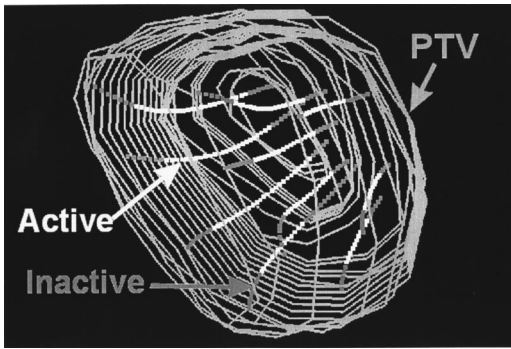


FIG. 9. 3D contour lines of the PTV for the breast implant.

method in clinical practice. This has enabled us to assess the accuracy of normal practice. The dose distribution is calculated assuming a $1/r^2$ dependence and ignoring any spatial anisotropy such as attenuation and any scattering effect. This is a reasonable approximation for this study.

We studied a high density of dose points per contour line, 4–10 points per cm, which were distributed uniformly on the PTV contour lines, see Figs. 7–11. The number of dose points used was in the range 665–2838, see Table I. We applied a *dose points only* optimization method and obtained a set of dwell position weights. Then we normalized these weights so that the average dose value on the PTV surface was equal to unity.

We choose *dose points only* optimization to estimate the dwell weights in order to be able to consider the case where the dose points have a maximum influence on the result so that we can achieve the best homogeneous dose distribution on the PTV surface.

The number of dose points uniformly distributed on the PTV contours or on the triangulated PTV surface according to our method were varied from 50 to 50 000 and corresponded to surface densities of dose points in the range 0.7–1200 points/cm².

The observed minimum dose value D_{\min} , maximum dose value D_{\max} , mean dose value D_{mean} and variance V_D based on the dose points generated by the classical contour based method (CB) using PTV contours and by our 3D surface based method (SB) on the PTV surface triangulation are shown in Figs. 12 and 13.

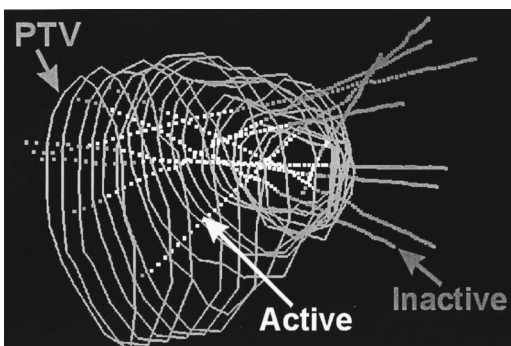


FIG. 10. 3D contour lines of the PTV for the cervix implant.

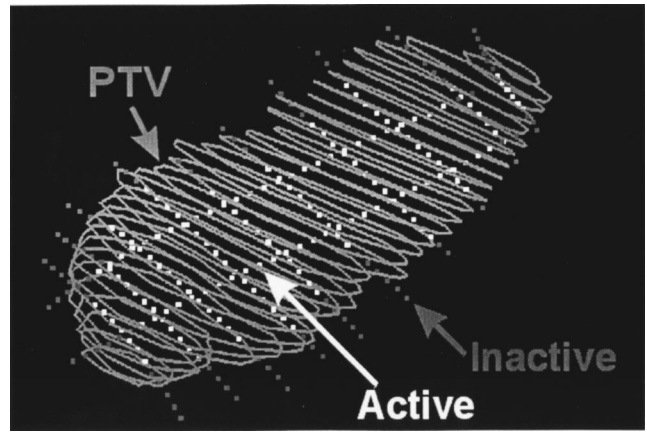


FIG. 11. 3D contour lines of the PTV for a rib metastases implant.

The parameters we used were selected to be representative of the dose distribution on the PTV surface. In our method we have taken into account the outer diameter of the metallic needles and flexible plastic catheters.

Table II gives the results of our comparison between the CB method with our new SB method, from which it is seen that the best agreement is achieved with D_{\min} but there can be wide discrepancies between the two methods for D_{\max} , D_{mean} , and V_D .

Figure 14 shows the dependence of (a) D_{\min} , (b) D_{\max} , (c) D_{mean} , and (d) V_D , calculated using our new SB method, on the density of sampling points for all five clinical implants. The results are normalized to the maximum surface dose point density. An accurate description of the true dose distribution on the PTV surface using our SB method can be achieved as follows. For D_{\min} a surface dose point density $>100/\text{cm}^2$, for $D_{\max} >50/\text{cm}^2$, for $D_{\text{mean}} >5/\text{cm}^2$ and for $V_D >100/\text{cm}^2$.

Figure 15 shows, using the breast implant as a representative example, $\text{PTV}=123.1 \text{ cm}^3$, that D_{\min} is very sensitive to user errors in mouse digitization and, therefore, great care should be taken in clinical practice if D_{\min} is to be used for dose prescription purposes. Indeed, in our opinion D_{\min} should not be used.

B. Catheters volumes

The following results have been obtained for the cervix implant using the optimization results, the dwell weights, obtained as previously described. We have calculated D_{\min} , D_{\max} , D_{mean} , and V_D within the PTV as a function of the number of sampling points inside the PTV, and the outer radius of the catheters. Our results are shown in Fig. 16.

As expected, D_{\min} is the same for all cases. The behavior of D_{\min} can be explained by the characteristic property of the quasi-random sequences, where successive points at any stage *know how to fill in the gaps* in the previously generated distribution. Therefore, by increasing the number of sampling points one of the sampling points will come closer to the minimum than does a sampling point in the previous case. But even for a dose point density of $500 \text{ points}/\text{cm}^3$

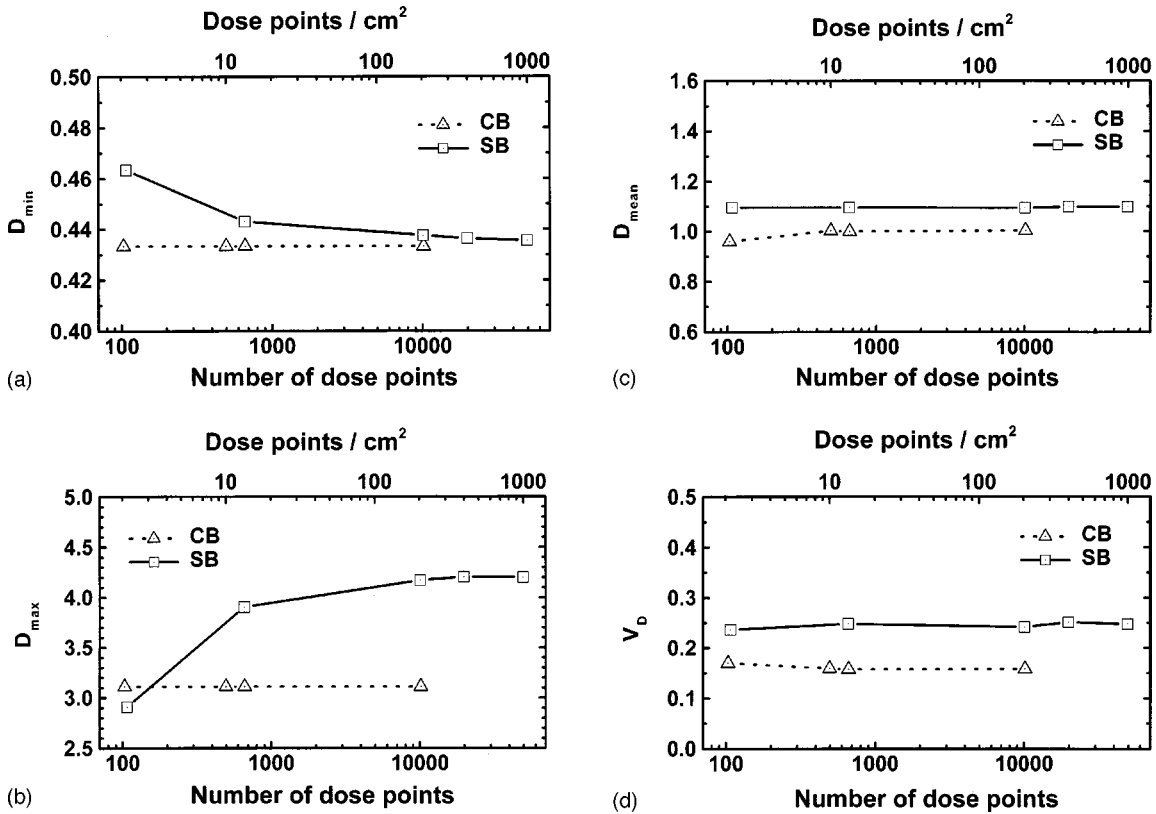


FIG. 12. Comparison for the prostate implant between results of the classical contour based method (CB) and of our new surface based method (SB) for (a) D_{min} , (b) D_{max} , (c) D_{mean} , and (d) variance V_D . The results are normalized.

corresponding to a mean grid size of 1.3 mm×1.3 mm×1.3 mm we can not be sure that the true minimum has been found, Fig. 16(a).

The same behavior is observed for D_{max} in the PTV, Fig. 16(b), although the sudden increase of D_{max} now depends on R . For $R=0$ mm there is no limitation on the D_{max} , whereas for $R=1$ mm and $R=2$ mm, D_{max} is reached after 20 000 sampling points. This corresponds to a volume dose point density of 90 points/cm³ which is a grid size of 2.2 mm×2.2 mm×2.2 mm.

For D_{mean} inside the PTV, Fig. 16(c) and for $R=1$ mm and $R=2$ mm, a smooth convergence to a limit is observed. D_{mean} for $R=0$ mm changes much more with the number of dose points and it increases suddenly when a new maximum dose value is reached. D_{mean} for $R=1$ mm reaches a limit at a density of 150 points/cm³ which is a grid size of 1.9 mm×1.9 mm×1.9 mm. For $R=2$ mm this limit is reached at a density of 30 points/cm³ which is a grid size of 3.2 mm×3.2 mm×3.2 mm.

For $R=0$ mm even at a density of 500 points/cm³ which is a grid size of 1.3 mm×1.3 mm×1.3 mm, no convergence is observed. D_{mean} for $R=1$ mm and $R=2$ mm lies within 5% of the convergence limit at a density of ~20 points/cm³ which is a grid size of 3.7 mm×3.7 mm×3.7 mm.

The variance of the dose values inside the PTV, V_D , is the quantity which is minimized in some dose optimization methods which attempt to reduce the dose inhomogeneity in the PTV. Whereas for $R=1$ mm and $R=2$ mm even with a

small number of sampling points a good approximation of the true dose variance is observed, for $R=0$ mm this quantity fluctuates in a similar way as D_{mean} . V_D for $R=1$ mm lies within 5% of the convergence limit at a density of ~90 points/cm³. For $R=2$ mm this is the case for a density of 50 points/cm³ which is a grid size of 2.7 mm×2.7 mm×2.7 mm. For $R=0$ mm even with a density of 500 points/cm³ no convergence is observed.

Our study shows that the rejection of dose points inside the catheters not only results in realistic dose distributions inside the PTV but in addition it reduces bias and numerical instabilities produced by dose points inside catheters.

In Table III the PTV volume is given for the five implants for the cases (a) where catheter volume inside the PTV is included, (b) where catheter volume ($R=1$ mm) is excluded, and (c) where catheter volume and an additional margin of 1 mm ($R=2$ mm) is excluded. For the clinical implants considered in our study the excluded volumes for $R=2$ mm are between 2% and 12%. This effect cannot be ignored in the 3D treatment planning procedure.

V. DISCUSSION AND CONCLUSIONS

Methods of producing dose points based on anatomical 3D information have been presented. The generation of dose points uniformly distributed on the surface of the PTV and not on the contours only, has shown that in general, more accurate D_{mean} , D_{min} , and D_{max} dose values on the surface

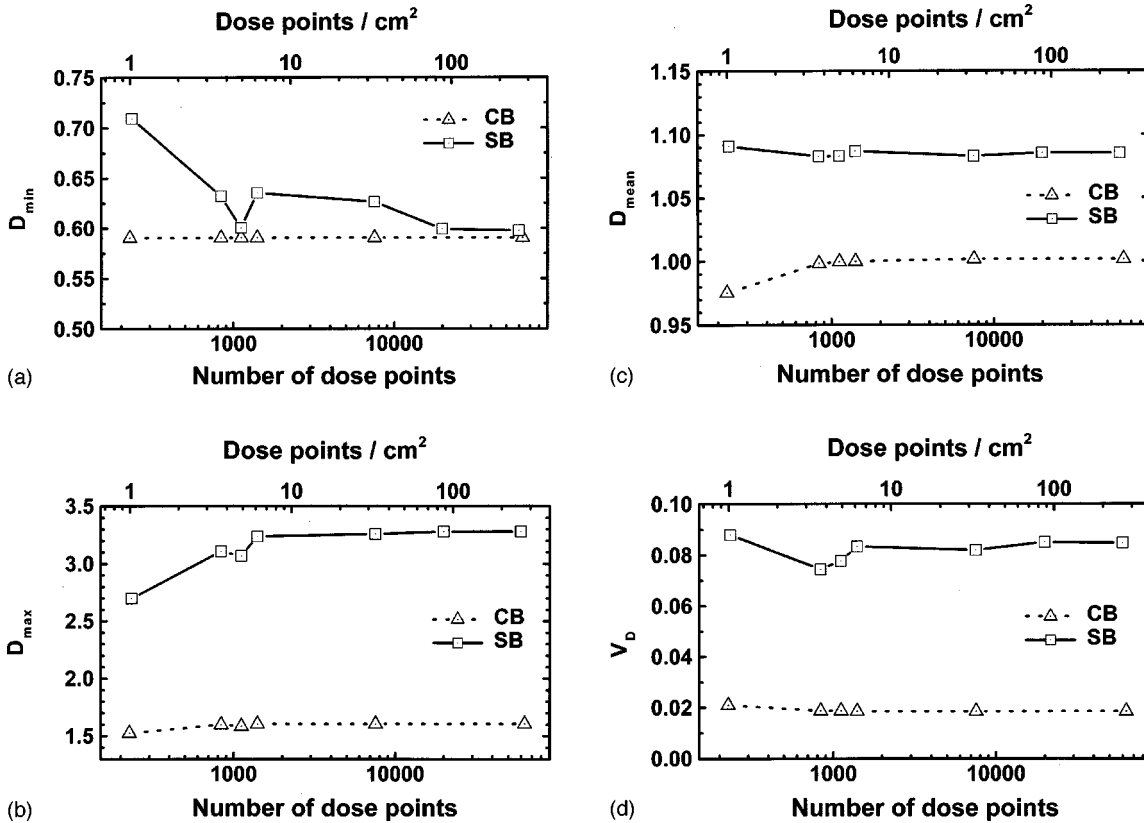


FIG. 13. Comparison for the cervix implant between results of the classical contour based method (CB) and of our new surface based method (SB) for (a) D_{min} , (b) D_{max} , (c) D_{mean} , and (d) variance V_D . The results are normalized.

of the PTV can be obtained. An improvement in the performance of the optimization methods which use V_D or other dose value parameters on the PTV surface can be expected in the future. These algorithms are relatively uncomplicated and require only a few additional seconds of computing time if the correct preprocessing has been made.

The dose distribution on the PTV surface, D_{mean} , D_{min} , D_{max} , and V_D for the whole surface are less biased than the corresponding values obtained using dose points limited to the contours of the PTV.

The D_{min} values of the CB method show a good agreement with our SB method. The slow convergence of D_{min} for the SB method suggests that the CB method is superior for the determination of D_{min} . This can be explained by the fact that some of the sampling points on the contours are on the convex hull of the surface and therefore their distance to the

source dwell points is maximum. Therefore, the minimum dose value is usually observed on one or more of these points. We could include these sampling points in the SB method but this would not eliminate problems such as contouring errors or source position inaccuracy which affects the D_{min} value more than it affects D_{mean} .

The concepts of dose prescription at the minimum target dose level (MTD) or minimum peripheral dose (MPD) are very sensitive for even small inaccuracies in the PTV contouring process. This is demonstrated in Fig. 15 where an error by the user in the mouse digitization process for a single contour point is simulated. Even an error of 3 mm in one contour line point results for this implant in a change of the D_{min} of 13%, Fig. 15(a). A pixel size of typically 0.5–1.0 mm corresponds to an error of 3–6 pixels in the image. In contrast, the estimated D_{mean} shows for a single contour point an error of 10 mm which is of less than 0.5%, Fig. 15(b). This indicates that such user entry errors do not significantly affect the value of D_{mean} . We have intentionally used an example of current clinical practice with the CB method as a demonstration. Figures 12 and 13 show that the same results are obtained using the SB method as with the CB method.

In addition to the problems which have been described, Yan Yu *et al.*²² have reported that D_{min} is very sensitive to the accuracy of the placement of seeds in permanent prostate implants. Because of these results we, therefore, do not recommend that D_{min} is used to describe the dose distribution.

TABLE II. Differences between the dose parameters on the PTV surface for the classical contour based method (CB) and our new surface based method (SB).

Implant site	D_{min} (%)	D_{max} (%)	D_{mean} (%)	V_D (%)
Neck	0.4	28.9	1.9	8.0
Prostate	0.5	35.0	9.4	56.1
Breast	1.4	1.0	0.1	8.6
Cervix	1.2	104.9	8.4	356.4
Rib	0.6	2.7	0.0	1.7

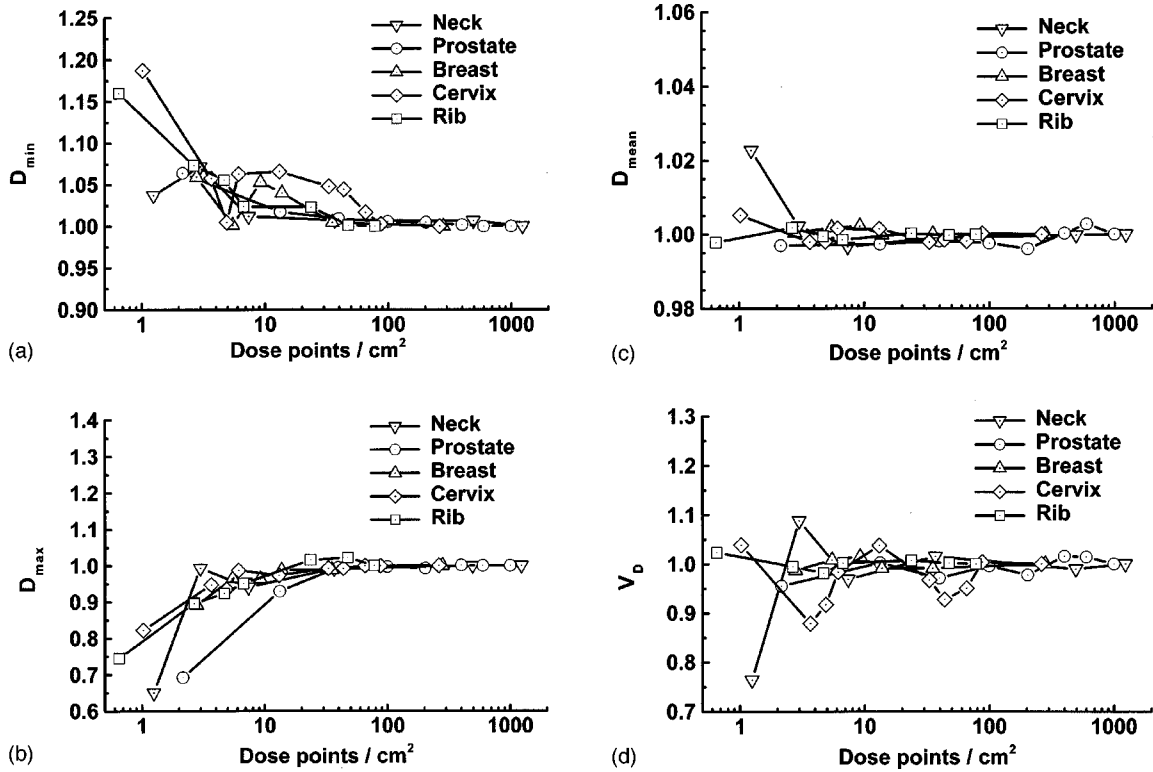


FIG. 14. Dependence of (a) D_{min} , (b) D_{max} , (c) D_{mean} , and (d) V_D calculated using the surface based method, on the density of sampling points for all five clinical implants. The results are normalized to the maximum surface dose point density.

On the other hand, the most stable behavior is demonstrated by D_{mean} when it is estimated on the true surface of the PTV. An accuracy of better than 1% is already achieved by surface dose point densities above 5 points/cm², see Fig. 14(c). Even if V_D convergences to a limit when the density is above 100 points/cm², both these parameters, D_{mean} and V_D , are from our study the optimum choice to document the dose in 3D-based treatment planning for brachytherapy.^{3,23} Our study also shows that single extreme values such as D_{min} and D_{max} are not appropriate to document or specify brachytherapy treatments.

For a comparison of the SB and CB methods we selected, using our autoactivation algorithm,¹⁵ only those sources which are at least 5 mm below the surface of the PTV. Without this constraint the differences between D_{mean} , D_{max} , and V_d for the SB and CB methods are even larger, possibly because some of the source dwells could be closer to the surface. This demonstrates that the SB method yields more accurate descriptions of the dose distribution on the surface of the PTV than the CB method.

The consideration of the catheter volumes and so the exclusion of sampling points inside the catheters removes the problems encountered by very high dose values from sampling points inside the catheters and leads to true anatomical dose distributions.

Our results for sampling densities within the PTV required for an acceptable accuracy, demonstrate that in contrast to the results for an optimum grid for external beam dose studies,^{1,2} where grid sizes of 5 mm×5 mm×5 mm, are

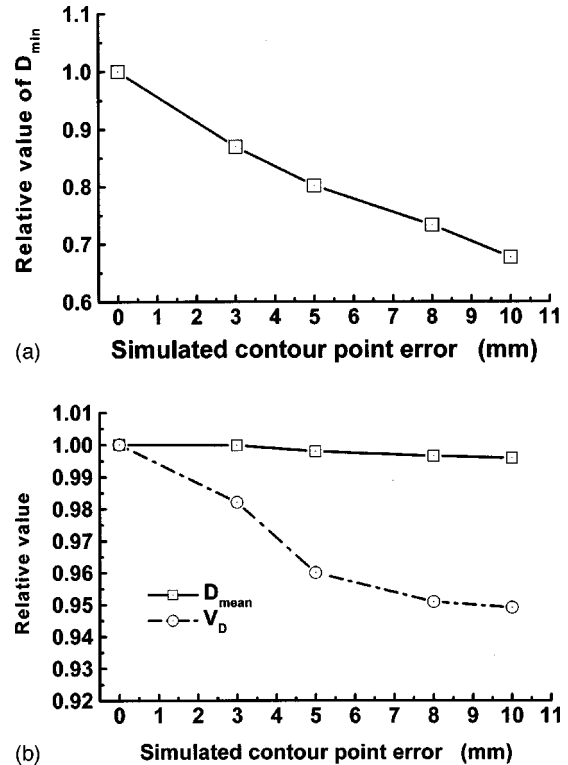


FIG. 15. Influence of mouse digitization error for a single PTV contour point for the breast implant. (a) D_{min} and (b) D_{mean} and V_D of the dose distribution calculated on the PTV surface using dose points only on contour lines. The values are normalized for cases without any digitization error.

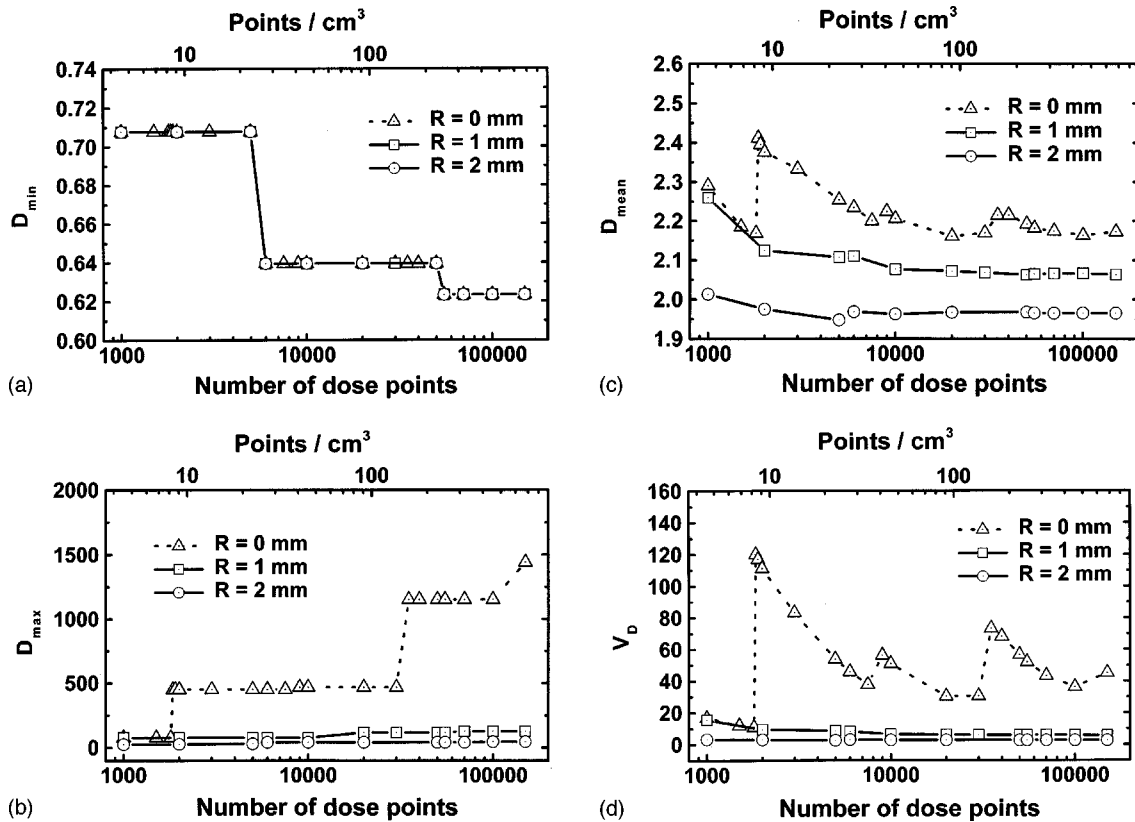


FIG. 16. Influence of the sampling size and sampling density for the dose points and of the catheter outer radius R on the calculated dose distribution inside the PTV for the cervix implant. (a) D_{\min} , (b) D_{\max} , (c) D_{mean} , and (d) V_D . Three cases for the radius R are considered.

reasonable. In brachytherapy, grid sizes of 1 mm×1 mm×1 mm can be required.

The analysis of the dose distributions within the PTVs is consistent with the results obtained for the PTV surface, in that D_{\min} and D_{\max} should not be used for dose optimization purposes.^{6,8,24} Only D_{mean} and V_D can be calculated with sufficient accuracy for dose optimization, where D_{mean} is usually indirectly used. These are the only two reliable parameters and we recommend that they are used in optimization procedures.

Current anatomy based optimization techniques are based on DVHs for PTV and normal tissues.³ DVHs are usually calculated from sampling points randomly distributed or from sampling points forming a regular grid. Random sampling points are preferentially used due to the problem that if the points are distributed on a regular grid then it is not possible to increase their number, i.e., reduce the grid size,

without the need to re-compute the DVHs. Uniformly random distributed points have the disadvantage of producing voids and clusters.

The use of deterministic *low-discrepancy sequences* (LDS), known as quasi-random sequences, avoids this problem.¹⁷ An important property is that they are spread out in a self-avoiding more uniformly distributed way. Since points from LDS do not use wasteful samples due to clusters and voids produced by uncorrelated random points, significantly fewer sampling points can be used in the Monte Carlo integration techniques using LDS instead of pseudo-randomly distributed points.^{1,2} Even using LDS, large sampling densities are required to accurately describe DVHs. The current dose optimization algorithms in clinical practice use 300–2000 dose points in the optimization process,^{3,4} otherwise optimization time would require many hours.

However, it should be realized that an accurate descrip-

TABLE III. Calculated PTV volumes and surface areas.

Implant site	PTV (cm ³)	PTV (cm ³)	PTV (cm ³)	Surface (cm ²)	Surface (cm ²)	Surface (cm ²)
	($R=0$ mm)	($R=1$ mm)	($R=2$ mm)	($R=0$ mm)	($R=1$ mm)	($R=2$ mm)
Neck	18.3	17.7	16.1	40.7	40.2	38.9
Prostate	21.0	20.7	19.9	50.3	49.7	48.2
Breast	125.1	123.1	117.2	142.4	141.6	139.4
Cervix	223.5	221.4	215.1	228.7	228.3	226.7
Rib	507.2	504.0	494.7	421.4	420.5	417.6

tion of the dose distribution requires of the order of 10^5 dose points. This is a computing time problem not only for the current algorithms but also for our multiobjective genetic optimization algorithm MOGA,³ which uses 10^5 dose points and is based on the optimization of the COIN distribution and the DVHs.³ A significant reduction of the sampling density has to be achieved because of these time constraints and, therefore, an optimum distribution of dose points must be determined. The sampling points must be distributed nonuniformly and adapted to the implant geometry and to the source dwell positions. However, there is a possible method of overcoming this time constraint problem using nonuniform distributed sampling points, but this has not been yet studied by any group.

ACKNOWLEDGMENTS

This work was partly supported by Grant No. (GRI-154-97) from the Federal Ministry for Education, Science, Research and Technology, International Bureau, German Aerospace Center Department (DLR), Bonn, Germany.

^{a)} Author to whom correspondence should be addressed. Telephone: +49-69-8405-4480; Fax: +49-69-8405-4481 or -864480. Electronic mail: mlahanas@gmx.de

¹ X.-Q. Lu and L. M. Chin, "Sampling techniques for the evaluation of treatment plans," *Med. Phys.* **20**, 151–161 (1993).

² X.-Q. Lu and L. M. Chin, Letters to the editor on "Further discussions on sampling methods—a response to Letters to the Editor [*Med. Phys.* **20**, 1375–1376 (1993)] and [*Med. Phys.* **20**, 1377–1380 (1993)]," **20**, 1381–1385 (1993).

³ M. Lahanas, D. Baltas, and N. Zamboglou, "Anatomy-based three-dimensional dose optimization in brachytherapy using multiobjective genetic algorithms," *Med. Phys.* **26**, 1904–1918 (1999).

⁴ E. K. Lee, R. J. Gallagher, D. Silvern, C.-S. Wu, and M. Zaider, "Treatment planning for brachytherapy: an integer programming model, two computational approaches and experiments with permanent prostate implant planning," *Phys. Med. Biol.* **44**, 145–165 (1999).

⁵ G. Yang, L. E. Reinstein, S. Pai, and Z. Xu, "A new genetic algorithm technique in optimization of permanent ¹²⁵I prostate implants," *Med. Phys.* **25**, 2308–2315 (1998).

⁶ Y. Yu and M. C. Schell, "A genetic algorithm for the optimization of prostate implants," *Med. Phys.* **23**, 2085–2091 (1996).

⁷ Y. Yu, "Multiobjective decision theory for computational optimization in radiation therapy," *Med. Phys.* **24**, 1445–1454 (1997).

⁸ Y. Yu, J. B. Y. Zhang, R. A. Brasacchio, P. G. Okunieff, D. J. Rubens, J. G. Strang, A. Soni, and E. M. Messing, "Automated treatment planning engine for prostate seed implant brachytherapy," *Int. J. Radiat. Oncol., Biol., Phys.* **43**, 647–652 (1999).

⁹ International Commission on Radiation Units and Measurements, "Dose and volume specification for reporting interstitial therapy," ICRU Report No. 58, Bethesda, MD, 1997.

¹⁰ H. Fuchs, Z. M. Kedem, and S. P. Uelson, "Optimal surface reconstruction from planar contours," *Commun. ACM* **20**, 693–702 (1977).

¹¹ J. D. Boissonnat and B. Geiger, "Three dimensional reconstruction of complex shapes based on the Delaunay triangulation," in *Proc. Biomedical Image Processing and Biomedical Visualization*, edited by R. S. Acharya and D. B. Goldof (SPIE, Bellingham, WA, 1993), pp. 964–979.

¹² A. Tsalpatouros, D. Baltas, C. Kolotas, C. Koutsouris, D. Uzunoglou, and N. Zamboglou, "CT based software for 3-D localization and reconstruction in stepping source brachytherapy," *IEEE Trans. Inf. Technol. Biomed.* **1**, 229–242 (1997).

¹³ R. Courant and H. Robbins, *What is Mathematics?* (Oxford University Press, New York, 1941).

¹⁴ H. Edelsbrunner and E. P. Mücke, "Simulation of Simplicity: A technique to cope with degenerate cases in geometric algorithms," *ACM Trans. Graphics* **9**, 66–104 (1990).

¹⁵ S. Giannouli, N. Milickovic, D. Baltas, M. Lahanas, N. Uzunoglu, and N. Zamboglou, "Autoactivation of source dwell positions: a new tool for imaging based HDR brachytherapy treatment planning," *STO-MEDPHYS Report*, 3-1999 (1999).

¹⁶ Y. Yu, "A non-divergent specification of the mean treatment dose in interstitial brachytherapy," *Med. Phys.* **23**, 905–909 (1996).

¹⁷ H. Press, S. A. Teukolsky, W. T. Vetterling, and B. P. Flannery, *Numerical Recipes in C*, 2nd ed. (Cambridge University Press, Cambridge, 1992).

¹⁸ M. Lahanas, D. Baltas, S. Giannouli, N. Milickovic, and N. Zamboglou, "Optimization of the bounding box of three-dimensional objects," *STO-MEDPHYS Report*, 2-2000 (2000).

¹⁹ M. Namiki and K. Fukuda, Unfolding 3-dimensional convex polytopes: a package for Mathematica 1.2 or 2.0. Mathematica Notebook, Univ. of Tokyo, (1993).

²⁰ Z. Michalewicz, *Genetic Algorithms + Data Structures = Evolution Programs* (Springer, Berlin, 1996).

²¹ J. E. Baker, "Reducing bias and inefficiency in the selection algorithm," edited by J. J. Grefenstette, *Genetic Algorithms and Their Applications: Proceedings of the Second International Conference on Genetic Algorithms* (Lawrence Erlbaum Associates, Hillsdale, NJ, 1987), pp. 14–21.

²² Y. Yu, F. M. Waterman, N. Suntharalingam, and A. Schulsinger, "Limitations of the minimum peripheral dose as a parameter for dose specification in permanent ¹²⁵I prostate implants," *Int. J. Radiat. Oncol., Biol., Phys.* **34**, 717–725 (1996).

²³ D. Baltas, C. Kolotas, K. Geramani, R. F. Mould, G. Ioannidis, M. Kekchidi, and N. Zamboglou, "A conformal Index (COIN) to evaluate implant quality and dose specification in brachytherapy," *Int. J. Radiat. Oncol., Biol., Phys.* **40**, 512–524 (1998).

²⁴ E. M. Messing, J. B. Y. Zhang, D. J. Rubens, R. A. Brasacchio, J. G. Strang, A. Soni, M. C. Schell, P. G. Okunieff, and Y. Yu, "Intraoperative optimized inverse planning for prostate brachytherapy: early experience," *Int. J. Radiat. Oncol., Biol., Phys.* **44**, 801–808 (1999).